Contents lists available at ScienceDirect

Applied Catalysis B: Environmental

Oxidative desulfurization of dibenzothiophene over monoclinic VO_2 phase-transition catalysts

Kun Chen [a,b], Ni Liu [b,c], Minghui Zhang [b,c,**], Danhong Wang [a,b,*]

[a] National Institute for Advanced Materials, School of Materials Science and Engineering, Nankai University, Tianjin 300350, China
[b] Key Laboratory of Advanced Energy Materials Chemistry (Ministry of Education), Collaborative Innovation Center of Chemical Science and Engineering (Tianjin), China
[c] College of Chemistry, Nankai University, Tianjin 300071, China

A B S T R A C T

Phase-pure monoclinic VO_2 (M) was successfully synthesized by hydrothermal reduction method using oxalic acid as a reductant and solvent-thermal reduction method using methanol as a reductant. Oxidative desulfurization (ODS) activities were investigated and the results revealed that intrinsic ODS activity increased with increasing cell volume for different synthesized VO_2 (M) catalysts. DSC measurement gives the evidence that phase transition temperature of monoclinic VO_2 (M) to rutile VO_2 (R) decreased with increasing cell volume for different VO_2 (M) catalysts. Variable-temperature *in-situ* Raman spectrum also confirmed that phase transition from VO_2 (M) to VO_2 (R) occurred. Mechanism of ODS reaction on VO_2 (M) catalyst was investigated precisely involving temperatures which phase transition occurred. Below the phase-transition temperature VO_2 (M) showed higher ODS reaction activation energy, while above the phase-transition temperature VO_2 (R) exhibited lower ODS activation energy. This result may be explained by the fact that V—O bond length for VO_2 (R) (1.93 Å) fits more for the five-member ring formed with the oxidant *tert*-butyl hydroperoxide (TBHP) during ODS reaction compared with V-O bond length for VO_2 (M) (about 2.03 or 1.86 Å).

© 2017 Elsevier B.V. All rights reserved.

1. Introduction

Recently, environmental problems have attracted much attention, many stringent regulations were published to restrict sulfur content in oils to ultra-low level (<10 ppm) [1,2]. In petroleum refining industry, hydrodesulfurization (HDS) is a conventional method to reduce sulfur, which is effective for removing non-thiophenic S-compounds such as thiols, sulfides, and disulfides. However, HDS is difficult to remove dibenzothiophenes (DBT) and its alkyl-substituted derivatives 4, 6-dimethydibenzothiophene (4, 6-DMDBT) owing to steric hindrance [3,4]. As a consequence, severe HDS reaction conditions (higher reaction temperatures and hydro-

gen pressures) are needed to achieve fuels with S concentration below 10 ppm, leading to increasing operation costs.

To obtain ultra-low sulfur fuels, alternative routes are developed, for example, catalytic oxidative desulfurization, adsorptive desulfurization, bio-desulfurization, extraction desulfurization, etc. ODS has attracted considerable interest due to mild reaction conditions such as lower reaction temperature, atmospheric pressure, converting sulfur-bearing molecules to sulfones and removing sulfones from oils by solvent extraction [5] or adsorption [6]. During last few decades, the application of ODS to liquid oils has been demonstrated to be very promising [7–11].

Lots of catalysts for ODS have been discussed in previous publications [11–15].

Currently, many publications reported V_2O_5 catalysts (V_2O_5/TiO_2 [16], V_2O_5/Al_2O_3 [17] and V_2O_5/AC [18]) showed high performances in the oxidation of sulfur-bearing molecules [19]. However, other vanadium oxides are still rarely studied for their ODS activities. In our previous study, we synthesized V_2O_3 nanoparticles using V_2O_5 as a precursor and methanol or oxalic acid as a reductant. V_2O_3 catalyst displayed a high ODS activity. For vanadium dioxide (VO_2), it is well known that monoclinic VO_2 (M) presents a structural transition to rutile VO_2 (R) at a

* Corresponding author at: National Institute for Advanced Materials, School of Materials Science and Engineering, Nankai University, Tianjin 300350, China and Key Laboratory of Advanced Energy Materials Chemistry (Ministry of Education), Collaborative Innovation Center of Chemical Science and Engineering (Tianjin), China.
** Corresponding author at: College of Chemistry, Nankai University, Tianjin 300071, China and Key Laboratory of Advanced Energy Materials Chemistry (Ministry of Education), Collaborative Innovation Center of Chemical Science and Engineering (Tianjin), China.
E-mail address: dhwang@nankai.edu.cn (D. Wang).

critical temperature of 68 °C. Low-temperature VO_2 (M) phase with a monoclinic $P2_1/c$ crystal system behaves as a semiconductor and high transmittance to near IR wavelengths, whereas high-temperature VO_2 (R) phase with a tetragonal P42/mnm crystal system exhibits as a metal and highly reflective to near IR wavelengths. This distinctive characteristic of VO_2 makes it a promising candidate for various technological applications. In fact, there were plenty of publications about vanadium dioxide VO_2 (M). Most of these publications studies on the technological applications such as thermochromic smart windows [20,21], IR uncooled bolometers [22], data storage media [23], etc. Little attention has been paid to their catalytic performance.

In recent years, it is reported solvothermal reduction methods can obtain VO_2 (M) with convenience. However, it is difficult to obtain pure VO_2 (M) and always doped with VO_2 (B) [24–26]. Therefore, the detailed conditions for solvothermal reduction methods were investigated and pure VO_2 (M) was obtained in this work. Moreover, it is very interesting that phase transition temperature of VO_2 (M) to VO_2 (R) is just in the range of ODS reaction temperatures, so it is very meaningful for us to focus on the elucidation of ODS mechanism when VO_2 (M) phase transition occurs. Due to the phase transition of VO_2 (M) to VO_2 (R), small distortion of the atomic lattice results in the change of V-O bond length. V-O bond is considered to act as the active site for ODS reaction. Therefore, in this work ODS activity studies involving phase transition temperature revealed the direct character of ODS mechanism occurred on VO_2 (M) and VO_2 (R) with different V-O bond length.

2. Experimental

2.1. Preparation of catalysts

2.1.1. Hydrothermal reduction method

Vanadium pentoxide and oxalic acid was dissolved in aqueous solution at 70 °C with stirring. A blue solution was obtained after 3 h. The solution was shifted into a 50 ml stainless-steel autoclave lined with Teflon, sealed and kept at 200 °C for 24 h. After lowering to room temperature, the precipitate was separated by filtering, then washed with deionized water and ethanol, and dried in air overnight. The precursor was treated in a tubular resistance furnace at 500 °C for 2 h in nitrogen atmosphere. VO_2 (M) powder was obtained after lowering to room temperature in nitrogen.

2.1.2. Solvent-thermal reduction method

In a typical synthesis procedure, one gram of V_2O_5 was directly added into a 50 ml stainless-steel autoclave lined with Teflon by the addition of excess methanol. The autoclave was sealed and kept at 180 °C for 12 h. Next steps were similar to the hydrothermal reduction method.

2.2. Characterization of catalysts

X-ray diffraction (XRD) patterns were obtained by CuKa radiation ($\lambda = 0.154178$ nm, tube voltage of 40 kV and tube current of 100 mA) in a Bruker D8 FOCUS from 10° to 80° (2θ) with a scanning rate of 6 (°)/min.

Surface areas were examined using BET method from N_2 adsorption isotherms recorded at 77 K using a Quantachrome Autosorb-iQ$_2$ apparatus. Before the measurements, the catalysts were dried for 4 h at 200 °C and degassed under vacuum for 24 h at 200 °C.

The differential scanning calorimetry (DSC) analysis was conducted on a TA SDT Q600 instrument. All catalysts were heated with a rate of 5 °C min^{-1} from ambient temperature to 100 °C using α-Al$_2$O$_3$ as the reference.

The Variable-temperature *in-situ* Raman spectrum of the composite samples were obtained using a Raman microscope in a RTS-HiR-AM from ambient temperature to 80 °C with a heat rate of 5 °C min^{-1} by a 532 nm laser source at an input power of 1 mW.

The morphologies of the samples were performed on a Nova NanoSEM digital scanning electron microscope (SEM) with a voltage of 2.0 kV and a current of 1.0 mA.

High-resolution TEM (HRTEM) images were acquired on a Philips Tecnai G2 F20 microscope with a voltage of 200 kV. The catalysts were dissolved in ethanol by ultrasound for 20 min, and then deposited a layer of catalysts on a copper grid.

2.3. Catalytic tests

VO_2 (M) powder was grinded to >200 mesh and used as the catalyst for ODS of dibenzothiophene (DBT). A simulated model oil (MD 500) was prepared as follows: 0.0505 g DBT was submerged in 100 g decalin to acquire 500 ppm DBT solution. And then, 0.1141 g *tert*-butyl hydroperoxide (TBHP) with the O/S (one oxygen atom in TBHP/one sulfur atom in DBT) molar ratio of 3.0 was mixed in the above solution. In ODS reaction, 10 g of model oil was added to a 50 ml round bottom flask, which was warmed to the reaction temperature with vigorous stirring, then 0.05 g catalyst was mixed in the solution, the ODS reaction continued for about 2 h. The quantification of oxidation products were conducted by means of GC2060 fitted out with a flame ionization detector (FID), using a 30 m * 0.32 mm ID AC1*0.25 μm film thicknes column and nitrogen as carrier gas.

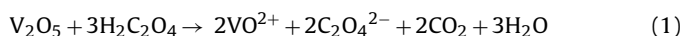## 3. Results and discussion

3.1. Synthesis of VO_2 (M)

3.1.1. Synthesis of VO_2 (M) using hydrothermal reduction method

Some factors can influence synthesis of VO_2 (M) powder using hydrothermal reduction method such as the amount of V_2O_5, molar ratio of oxalic acid to V_2O_5, hydrothermal temperature, hydrothermal time, crystallization temperature and crystallization time. Fig. 1 showed XRD patterns of the catalysts synthesized by hydrothermal reduction method at various conditions. All experiments were carried out by changing one of the following basic conditions: amount of V_2O_5 with 12.5 mg/ml, molar ratio of oxalic acid to V_2O_5 of 3:1, hydrothermal temperature at 200 °C, hydrothermal time for 24 h, crystallization temperature at 500 °C and crystallization time for 2 h. Under most conditions pure VO_2 (M) can be obtained from XRD results. Most of the peaks for those impure samples can be assigned to VO_2 (M) (JCPDS 43-1051, $a = 5.752, b = 4.538, c = 5.383, \beta = 122.64°, d_{011} = 3.207$ Å) except XRD peak of 2θ at 25°, which corresponds to the main peak of VO_2 (B) (JCPDS 65-7960) [27].

The synthesis process was initiated by reducing V_2O_5 in the presence of oxalic acid to vanadyl oxalate (VOC_2O_4) when vanadium pentoxide and oxalic acid was dissolved in aqueous solution at 70 °C with stirring. A blue solution was obtained after 3 h indicating the formation of V^{4+} as VOC_2O_4 [24]. The formation of VO_2 crystals occurred during the subsequent hydrothermal step with the decomposition of VOC_2O_4. The obtained VO_2 precursor was characterized to be VO_2 (B) (JCPDS 65-7960) by XRD results and VO_2 (B) converted to VO_2 (M) with subsequent crystallization at ≥ 500 °C in nitrogen (Fig. 1e). The VO_2 formation is summarized by the chemical reaction equation (1) (2) (3) [24,28].

$$V_2O_5 + 3H_2C_2O_4 \rightarrow 2VO^{2+} + 2C_2O_4{}^{2-} + 2CO_2 + 3H_2O \tag{1}$$
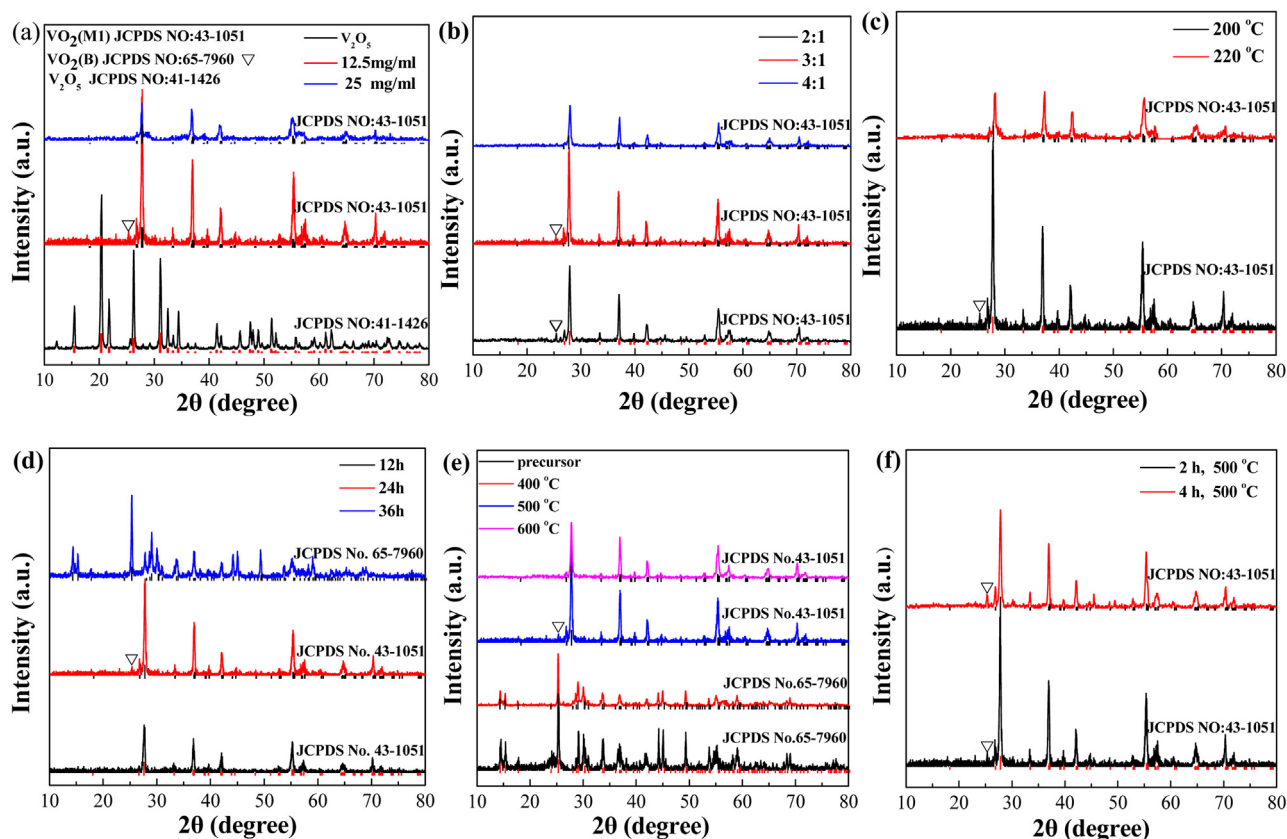
$$VOC_2O_4 \rightarrow VO_2(B) + CO_2 + CO \tag{2}$$

Fig. 1. XRD spectra collected from VO$_2$ samples synthesized under different conditions using hydrothermal reduction method. (a) amount of V$_2$O$_5$ with 12.5 or 25 mg/ml. (b) molar ratio of oxalic acid to V$_2$O$_5$ of 2:1, 3:1 or 4:1. (c) hydrothermal temperature at 200 or 220 °C. (d) hydrothermal time for 2 or 4 h. (e) precursor and crystallization temperature at 400, 500 or 600 °C. (f) crystallization time for 2 or 4 h.

$$VO_2(B) \xrightarrow[>500^oC]{N_2} VO_2(M) \qquad (3)$$

According to Fig. 1, we can concluded that the following conditions were appropriate to convert VO$_2$ (B) precursor into VO$_2$ (M) product: higher concentration of vanadium pentoxide with 25 mg/ml, higher molar ratio of oxalic acid to vanadium pentoxide of 4:1, higher hydrothermal temperature at 220 °C, shorter hydrothermal time for 12 h, higher crystallization temperature at 600 °C and shorter crystallization time for 2 h. Pure VO$_2$ (M) can be obtained under these conditions.

3.1.2. Synthesis of VO$_2$ (M) using solvent-thermal reduction method

With solvent-thermal reduction method, all experiments were carried out by changing one of the following basic conditions: 1 g of V$_2$O$_5$ was dissolved in 30 ml methanol at 180 °C for 12 h, then filtered, washed and crystallized at 500 °C in N$_2$ atmosphere for 2 h. The influence factors, such as the amount of V$_2$O$_5$, solvent-thermal temperature and time, crystallization time were considered to obtain pure VO$_2$ (M). Fig. 2 discribed XRD patterns of the catalysts synthesized by solvent-thermal reduction method at different conditions. Pure VO$_2$ (M) (JCPDS 43-1051) can be obtained at most different conditions. According to Fig. 2 the appropriate conditions to obtain pure VO$_2$ (M) with good monoclinic structure are as following: appropriate amount of vanadium pentoxide of 1 g, lower hydrothermal temperature at 160 °C, shorter crystallization time for 2 h and shorter hydrothermal time for 12 h.

Using silver mirror reaction, aldehyde products were examined to be formed in the solution after solvent-thermal procedure. The formation of VO$_2$ (M) crystals occurred after the subsequent crystallization step and was summarized by the chemical reaction Eq. (4).

$$V_2O_5 + CH_3OH \rightarrow 2VO_2(M) + HCHO + H_2O \qquad (4)$$

Although pure VO$_2$ (M) was obtained by solvent-thermal reduction method as discussed above, a second-order phase transition was detected by DSC curve in Fig. 3a. VO$_2$ (M) sample crystallized at 500 °C for 2 h in N$_2$ atmosphere showed no specific phase transition temperature. It became complicated for us to investigate the phase transition effect on ODS activity. Therefore, synthesis conditions for solvent-thermal reduction method are further studied. Fortunately, a first-order phase transition VO$_2$ (M) sample was obtained when crystallized at 500 °C for 5 h in argon atmosphere. This result was identified by DSC curve in Fig. 3a. Fig. 3b showed XRD results, all the peaks of the two samples were assigned to VO$_2$ (M) (JCPDS 43-1051). Based on these results, it was easy for us to synthesize first- or second-order phase transition VO$_2$ (M) catalyst.

Among the synthesized pure VO$_2$ (M) under different conditions as obtained in Figs. 1 and 3 with the same monoclinic structure (M1), obvious XRD peak shifts are observed for four samples as shown in Fig. 4. Using XRD analysis software of Jade, lattice parameters of the synthesized catalyst VO$_2$ (M1) were calculated and shown in Table 1. When the main XRD peak (27.8°) shifts to higher degree as shown in Fig. 4b, the calculated cell volume of VO$_2$ (M) decreases in the order VO$_2$ (1) > VO$_2$ (2) > VO$_2$ (3) > VO$_2$ (4). Higher molar ratio of oxalic acid to vanadium pentoxide of 4:1 and higher hydrothermal temperature at 220 °C using hydrothermal reduction method caused cell contraction of synthesized VO$_2$ (M). The decrease in cell volume also means the decrease in V—O bond which will affect the ODS activity discussed consequently.
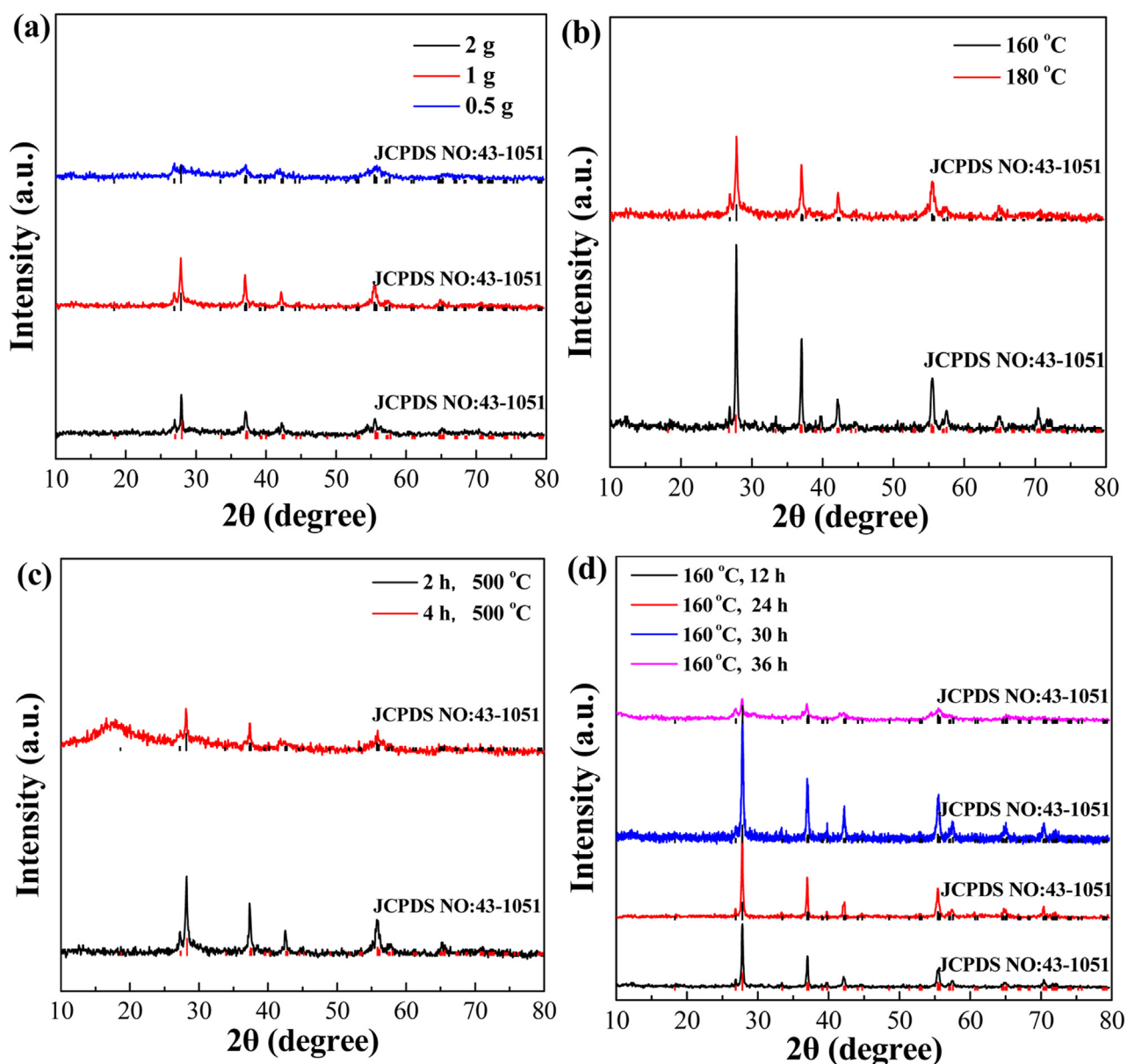
Fig. 2. XRD data collected from VO$_2$ samples synthesized under different conditions using solvent-thermal reduction method. (a) amount of V$_2$O$_5$ with 2, 1 or 0.5 g. (b) solvent-thermal temperature at 160 or 180 °C. (c) crystallization time for 2 or 4 h at 500 °C in N$_2$ atmosphere. (d) solvent-thermal time for 12, 24, 30 or 36 h with solvent-thermal temperature at 160 °C.
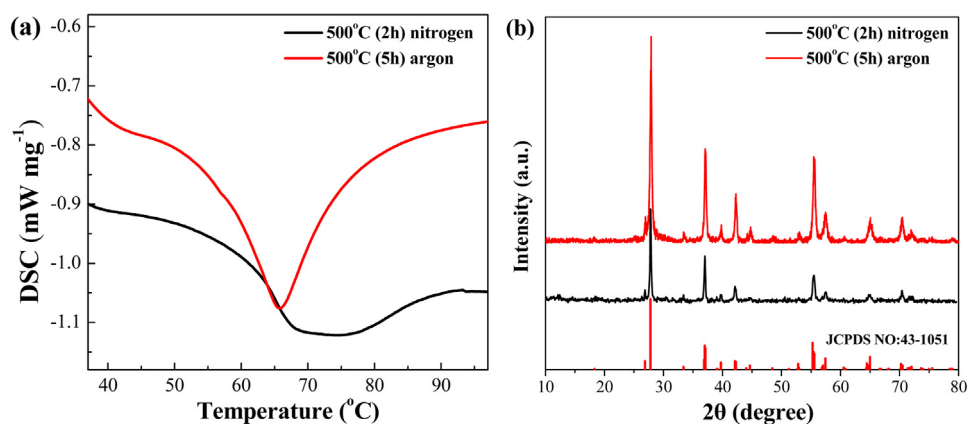

Fig. 3. (a) DSC results for VO$_2$ samples crystallized at 500 °C for 2 h in N$_2$ atmosphere (solvent-thermal temperature 160 °C) or crystallized at 500 °C for 5 h in argon atmosphere (solvent-thermal temperature 180 °C) by solvent-thermal reduction methods. (b) XRD data for the two samples.
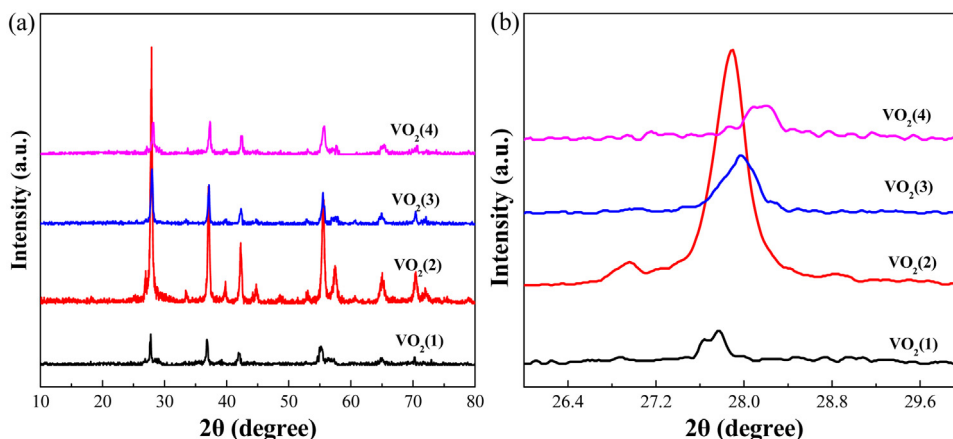
Fig. 4. (a) XRD data collected from VO_2 samples synthesized under different conditions using hydrothermal reduction method and solvent-thermal reduction method. (b) Amplification of the main peak ($2\theta = 27.8°$).

Table 1
Lattice constants for the synthesized pure VO_2 (M1) under different conditions with the same monoclinic structure.

catalyst	reductant (conditions)	a	b	c	β	V
$VO_2(1)$	oxalic acid(25 mg/ml)	5.742	4.576	5.373	123.05	118.33
$VO_2(2)$	methanol(argon)	5.740	4.524	5.358	122.59	117.23
$VO_2(3)$	oxalic acid(4:1)	5.623	4.536	5.198	120.56	114.16
$VO_2(4)$	oxalic acid(220 °C)	5.568	4.552	5.093	120.12	111.65

*$VO_2(1)$: with oxalic acid as reductant and V_2O_5 amount of 25 mg/ml, $VO_2(2)$: with methanol as reductant and crystallization at 500 °C for 5 h in argon atmosphere, $VO_2(3)$: with oxalic acid as reductant and molar ratio of oxalic acid to V_2O_5 4:1, $VO_2(4)$: with oxalic acid as reductant and hydrothermal temperature at 220 °C.

3.2. Oxidative desulfurization on VO_2 (M) catalyst with different cell volume

Two samples with high cell volume obtained in Table 1 were selected (VO_2 (1) and VO_2 (2)) to compare their intrinsic ODS activities. BET, SEM, HRTEM, variable-temperature Raman spectrum and DSC are also used to characterize the structure and properties of the two VO_2 (M) samples. This two kinds of VO_2 (M) were evaluated as ODS catalysts and presented different ODS activities for DBT as shown in Fig. 5.

Fig. 5 shows the catalytic performance of VO_2 (1) in comparison with VO_2 (2) for ODS of DBT. VO_2 (2) showed higher DBT conversion than VO_2 (1) from the results. Homologously, the BET surface areas for VO_2 (1) and VO_2 (2) were 1 m^2/g and 17 m^2/g, respectively. According to the calculation formula of TOF (TOF = $n/(m^*t)$, where n is the mole of reacted DBT molecular per gram catalyst, and m is the mole of surface active site VO_2 per gram catalyst, t is reaction time), VO_2 (1) showed higher TOF value than VO_2 (2), which means that VO_2 (1) presents higher intrinsic ODS activity than VO_2 (2). This may be explained by the fact that VO_2 (1) presents higher cell volume than VO_2 (2) as obtained in Table 1. Moreover, we have reported that the order of TOF values for mesoporous silica catalysts was $10^{-5} S^{-1}$, which was two orders lower than that for VO_2 (M) catalyst, indicated that VO_2 (M) shows much higher intrinsic ODS activity than mesoporous silica [29].

Morphology of VO_2 (M) samples was investigated. SEM images illustrated sheets-like morphology for VO_2 (1) (Fig. 6a), VO_2 (2) (Fig. 6b) and VO_2 (4) (Fig. 6c). From HRTEM results (Fig. 6d–f), the sheets displayed clear lattice fringes and crystalline structures. The inter-plane distance was calculated to be around 0.3256 nm for VO_2 (1), 0.3163 nm for VO_2 (2) and 0.3111 nm for VO_2 (4).which matches well with the spacing of two (011) crystal planes for VO_2 (M) (JCPDS 43-1051, d_{011} = 3.207 Å) [30,31]. The inter-plane distance decreased

in the order VO_2 (1) > VO_2 (2) > VO_2 (4), which was consistent with the results obtained by XRD in Fig. 4b. The main XRD peak (011) shifts to higher degree, which means the inter-plane distance (011) decreases.

In our synthetic system for hydrothermal reduction method, it was very significant for the formation of VOC_2O_4 precursor, which might act as a template for VO_2 sheets formation. The $C_2O_4^{2-}$ is deduced to serve as a bidentate ligand in the solution forming a complex precursor as shown in Fig. 7. In the precursor, VO^{2+} ions with tetravalent vanadium were bonded with two $C_2O_4^{2-}$ ions to form a planar molecule. These complexes further constructed into plate-like VO_2 during hydrothermal procedure [32].

Zou et al. reported that VO_2 (M) particles were composed by thermal decomposition of a $VO(C_2H_4O_2)$ precursor with tetravalent vanadium in air [25]. Similarly, in our synthetic system for solvent-thermal reduction method, methanol served as not only the reductant but also the template, and $VO(CH_3O)_2$ precursor with tetravalent vanadium may be also formed to further construct into plate-like VO_2, as shown in SEM image.

The phase transition behaviors of VO_2 (M) samples were clearly detected by DSC curves in Fig. 8a. The performance of endothermic peak shows the occurrence of structural phase transition from monoclinic VO_2 to tetragonal VO_2. The results demonstrated that first-order phase transition occurred for VO_2 samples and phase transition temperature increased in the order VO_2 (1) (65 °C) < VO_2 (2) (66 °C) < VO_2 (4) (68 °C) [30]. Moreover, the distinct structural transition from VO_2 (M) to VO_2 (R) was further confirmed by the variable-temperature *in-situ* Raman spectra for VO_2 (1) sample as shown in Fig. 8b. The Raman spectra peaks obtained at lower temperatures (<65 °C) with 192, 220 and 627 cm^{-1} is assigned to VO_2 (M) [26,33]. The frequency peaks at 192, 220 and 627 cm^{-1} are assigned to be V–V pairing vibrations, V–V tilting vibrations and V-O vibrations, respectively. Along with increasing temperatures (>65 °C), the Raman peaks disappear gradually by transition into the VO_2 (R) phase. The phase transition temperature obtained by Raman spectra is very consistent with the DSC result for VO_2 (1) sample. Different phase transition temperature for VO_2 samples may be explained by different cell volume, which leads to different cell tightness. When the cell volume decreased in the order VO_2 (1) < VO_2 (2) < VO_2 (4), the phase transition temperature increased.

3.3. Effect of phase transition on ODS activity using VO_2 (M) catalyst

As obtained above, VO_2 (M) presents an insulator-metal transition at a temperature of about 68 °C with a structural conversion
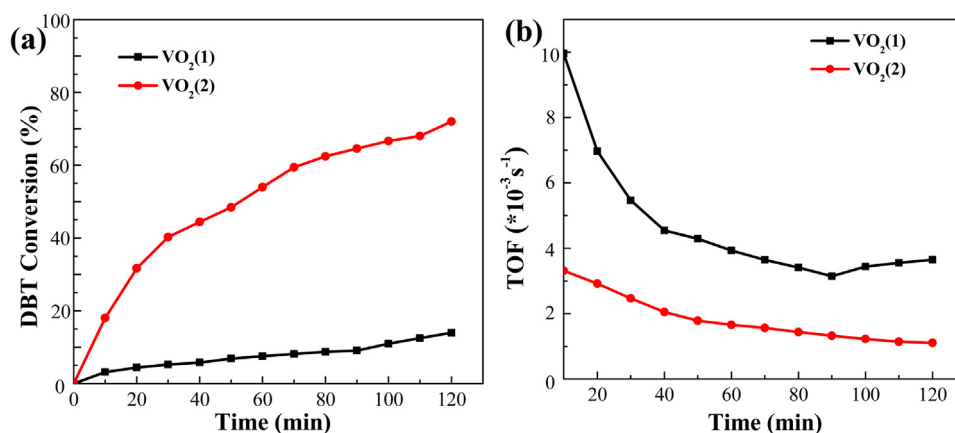
Fig. 5. (a) DBT Conversion on VO$_2$ (1) and VO$_2$ (2) with O/S molar ratio of 3.0 at 60 °C. (b) Calculated TOF values for VO$_2$ (1) and VO$_2$ (2).
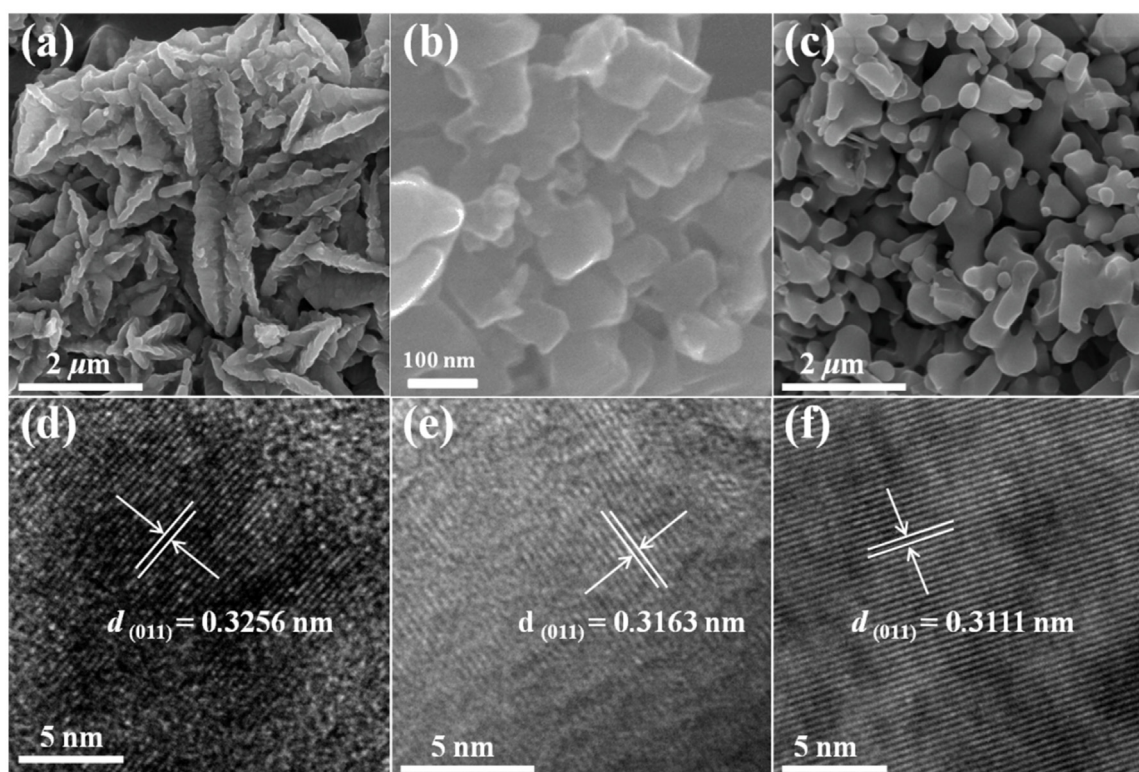

Fig. 6. (a) SEM and (d) HRTEM for VO$_2$ (1). (b) SEM and (e) HRTEM for VO$_2$ (2). (c) SEM and (f) HRTEM for VO$_2$(4).
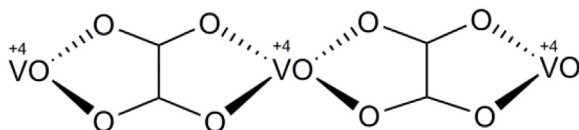

Fig. 7. Schematic image of metal oxalate complex VOC$_2$O$_4$.

from a low-temperature VO$_2$ (M) phase (Fig. 9a) to a high-temperature VO$_2$ (R) phase (JCPDS 79-1655, $a = b = 4.554$, $c = 2.856$, $\beta = 90°$, $d_{110} = 3.220$ Å) (Fig. 9b) [34]. There are four VO$_2$ molecules in VO$_2$ (M) unit cell and two VO$_2$ molecules in VO$_2$ (R) unit cell. Vanadium atom is octahedral coordinated with six oxygen atoms (VO$_6$ octahedra) for VO$_2$ (M) and VO$_2$ (R). Zigzag V^{4+}-V^{4+} pairs in VO$_2$ (M) change to infinite V^{4+}-V^{4+} linear chains in VO$_2$ (R) during phase transition. VO$_2$ (2) sample shows high DBT conversion due to

its high surface area (17 m^2/g), we adopted this VO$_2$ (M) catalyst to investigate phase transition effect on oxidative desulfurization. The oxidative reaction of model sulfur compound DBT was conducted at 66 °C, 68 °C, 70 °C, 72 °C, 74 °C, 76 °C, 78 °C, 80 °C and 82 °C on VO$_2$ (2) under the same reaction conditions.

The ODS activities of VO$_2$ (M) at different temperatures were summarized in Fig. 10. Normally, ODS activity increased with increasing reaction temperature. It is no difficult to find that ODS activity appeared something abnormal at reaction temperature of 76 °C. Phase transition between VO$_2$ (M) and VO$_2$ (R) may be occurred at the apparent transition temperature of 76 °C. A deep process was observed for ODS activity at the apparent phase transition temperature, indicating that phase transition of bulk VO$_2$ greatly affected ODS reaction on the surface active sites of catalyst.

The internal and external diffusion of the catalysts can be eliminated by reducing the particles size (grinded to >200 mesh)
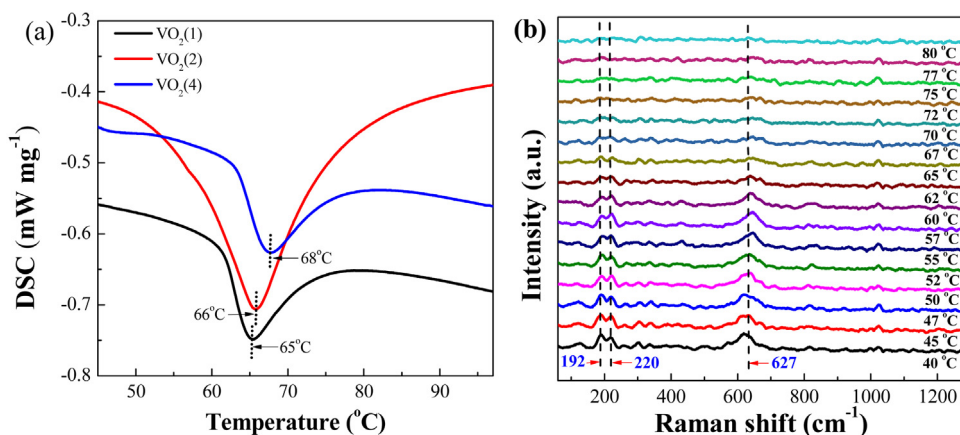
Fig. 8. (a) DSC results for VO$_2$ (1), VO$_2$ (2), VO$_2$ (4). (b) variable-temperature *in-situ* Raman spectrum for VO$_2$ (1).
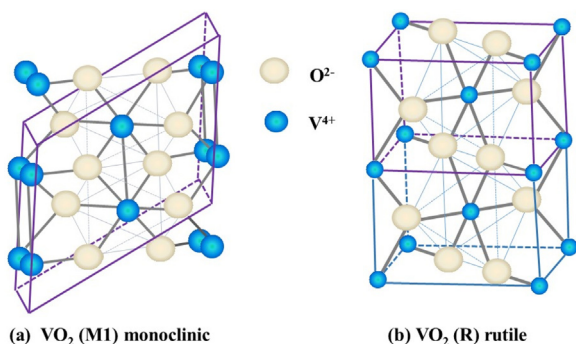

Fig. 9. Unit cell (marked by purple line) for VO$_2$ (M) and VO$_2$ (R).

and increasing the reaction stirring speed. The above experiments excluded the influence of the two factors. The results in Fig. 11 reveals that a linear relation of $ln(c_0/c)$ with reaction time (t) was acquired on VO$_2$ (M). Here c_0/c was defined as initial sulfur (DBT) concentration/unreacted sulfur (DBT) concentration. Therefore, the following equation applies: $ln\,(c_0/c) = k_{ODS}\,t$, where $k_{ODS} = A\,exp\,(-E_a/RT)$, here E_a is the apparent activation energy, A is the pre-exponential factor, T and R are the reaction temperature and gas constant, respectively. Therefore, from the slopes of $ln(c_0/c) \sim t$ lines, the reaction rate constants k_{ODS} at different temperatures can be obtained. The results demonstrated that ODS reaction of DBT can
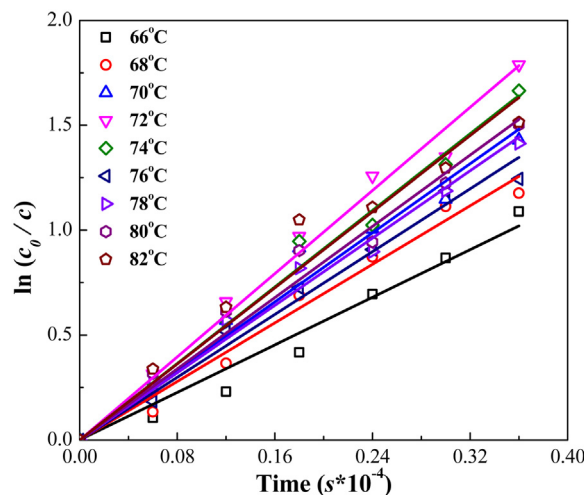

Fig. 11. Pseudo first-order reaction for oxidation of DBT on VO$_2$ (2).

be regarded as a pseudo first-order reaction. The slope parameters are listed in Table 2.

Fig. 12 illustrated the Arrhenius plots for oxidation of DBT on VO$_2$ (2) catalyst according to k_{ODS} at various temperatures. The apparent activation energies of ODS reaction were calculated from the slopes of $ln(k_{ODS}) \sim T$ lines. The consequences revealed that the activation energies were very different before and after phase tran-
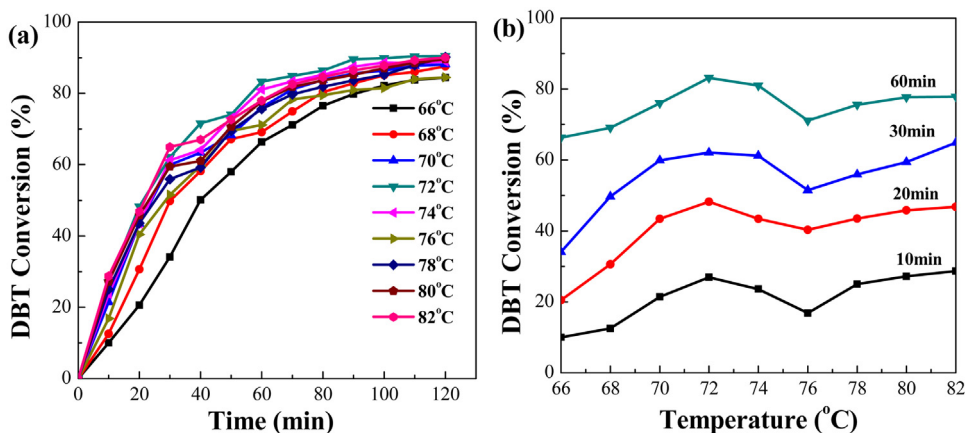

Fig. 10. (a) DBT conversion on VO$_2$ (2) with reaction time at different temperatures in a batch reactor. Reaction conditions: 10 g MD 500, 0.05 g VO$_2$ (M), O/S = 3:1. (b) DBT conversion on VO$_2$ (2) with reaction temperature at different time.

Table 2
Reaction rate constants (k_{ODS}) at various temperatures. Reaction conditions: 10 g MD 500, 0.05 g VO$_2$ (2), O/S = 3:1.

T/°C	$k_{ODS}/10^{-4} s^{-1}$	R^2
66	2.83	0.99
68	3.49	0.99
70	4.11	0.99
72	4.96	1.00
74	4.56	0.99
76	3.74	0.99
78	4.01	0.99
80	4.24	0.99
82	4.53	0.99
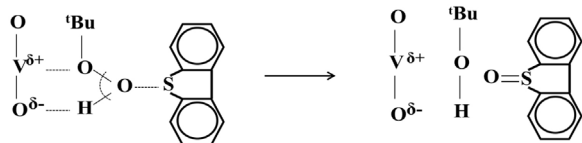
Scheme 1. Mechanism of surface-mediated oxidation procedure over VO$_2$.
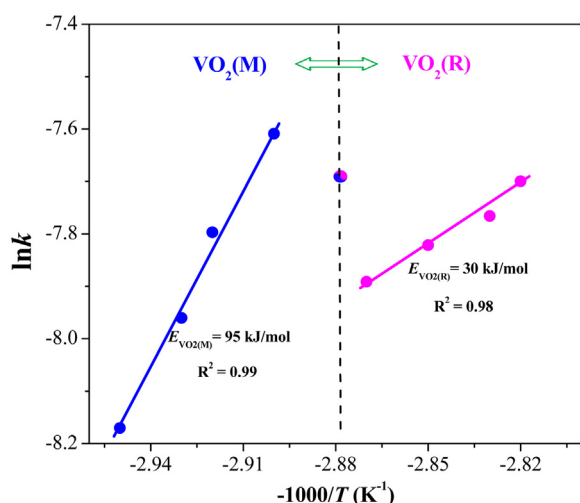
Fig. 12. Arrhenius plots for oxidation of DBT on VO$_2$ catalyst.

sition. Before phase transition at low reaction temperature, E_{a1} is equal to 95 kJ/mol for VO$_2$ (M). After phase transition at high reaction temperature, E_{a2} is equal to 30 kJ/mol for VO$_2$ (R) [7,11,35–37]. From this important result, it is suggested that there is difference in the mechanism for ODS of DBT catalyzed on VO$_2$ (M) and VO$_2$ (R) catalysts.
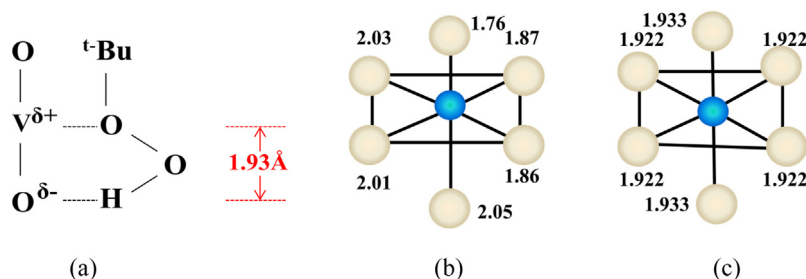
3.4. ODS mechanism on VO$_2$ (M) and VO$_2$ (R)

In our previous study [38], we proposed ODS mechanism of DBT on MoO$_3$ with TBHP according to Mashio's research [39]. Mashio et al. supposed the model at the initial stage of the complex formation between hydroperoxide and MoO$_3$. The distance between Mo atom and oxygen atom of MoO$_3$ is 1.96 Å, and the distance between oxygen atom adjacent to *tert*-butyl group and hydrogen atom of TBHP is 1.93 Å. Good agreement with atom distance is observed and a five member ring is formed due to the coordination of hydroperoxide to Mo-O. This coordination is prompted by the polarization of Mo$^{\delta+}$-O$^{\delta-}$ bond, and therefore, the electrophilicity of peroxy oxygen is prompted. Similarly, we proposed that a five-member ring formed on VO$_2$ with TBHP. Scheme 1 illustrated ODS mechanism of DBT on VO$_2$ catalyst. V-O bond acts as the active site and a five-member ring is formed with the absorption of TBHP. The crystal structure of VO$_2$ (M) and VO$_2$ (R) exhibited VO$_6$ distorted octahedral with V-O bond length as illustrated in Scheme 2b (VO$_2$ (M) 2.01, 2.03,2.05, 1.76, 1.87 and 1.86 Å) and Scheme 2c (VO$_2$ (R) 1.933, 1.933, 1.922, 1.922, 1.922 and 1.922 Å) [30,40–42]. The bond length between vanadium atom and oxygen atom of VO$_2$ (R) is 1.922 and 1.933Å, which very fits for the distance between hydrogen atom and oxygen atom of TBHP 1.93 Å as illustrated in Scheme 2a. The polarization of V$^{\delta+}$-O$^{\delta-}$ bond prompted the coordination of hydroperoxide with V-O to form a five-member ring. The sulfur atom of DBT attacked oxygen atom leading to the formation of DBT sulfoxide and *tert*-buthanol. This is good accordance with the former conclusion: VO$_2$ (R) showed lower ODS reaction activation energy activation energy (E_a) than VO$_2$ (M), which can be verified by the fact that VO$_2$ (R) better fits for the five-member ring during ODS reaction than VO$_2$ (M).

As discussed in Fig. 5, VO$_2$ catalysts show two orders higher TOF values than pure mesoporous silicas that we reported previously [29]. This result may be explained by that V-O active site shows higher intrinsic activity than surface silanol active site O—H. Because the bond length of V-O is longer than that of O—H (about 1 Å), which better fits for the five-member ring during ODS reaction as shown in Scheme 2a. Moreover, as obtained in Fig. 5, the VO$_2$ (M) catalysts with lower cell volume shows lower intrinsic ODS activity. Lower cell volume will lead to shorter V-O bond length for VO$_2$ (M) as shown in Scheme 2b. Therefore, it is assumed that shorter V-O bond length for VO$_2$ (M) results in lower intrinsic ODS activity.

4. Conclusions

In summary, we successfully synthesized phase pure VO$_2$ (M). Our findings revealed that applying the phase transition effect on VO$_2$ (M) catalyst might make progress in regulating ODS activation energy *in-situ*, with promising prospect for designing new phase-transition catalysts by active control of the bond length. The main results of this work can be summarized as follows:

Scheme 2. (a) The coordination of hydroperoxide to V-O on VO$_2$ catalyst and peroxidic oxidation mechanism of DBT with TBHP. (b) bond length of VO$_2$ (M). (c) bond length of VO$_2$ (R).

1. Intrinsic ODS activity increased with increasing cell volume on different VO_2 (M) catalysts with the same monoclinic structure due to increasing V-O bond length.
2. Phase transition temperature between VO_2 (M) and VO_2 (R) decreased with increasing cell volume for VO_2 (M) catalysts, which can be explained by the fact that the distortion of V-O bond can be easily occurred with high cell volume.
3. VO_2 (R) showed lower ODS reaction activation energy (E_a) than VO_2 (M), which could be attributed to the fact that V-O bond length (1.93 Å) of VO_2 (R) better fits for the five-member ring formed during ODS reaction than that of VO_2 (M).

Acknowledgments

References

[1] J. Eßer, P. Wasserscheid, A. Jess, Green Chem. 6 (2004) 316–322.
[2] O. Kröcher, M. Widmer, M. Elsener, D. Rothe, Ind. Eng. Chem. Res. 48 (2009) 9847–9857.
[3] C. Song, X.L. Ma, Appl. Catal. B 41 (2003) 207–238.
[4] H. Lu, J. Gao, Z. Jiang, Y. Yang, B. Song, C. Li, Chem. Commun. 2 (2007) 150–152.
[5] Y. Tian, Y. Yao, Y. Zhi, L. Yan, S. Lu, Energy Fuels 29 (2015) 618–625.
[6] O. Etemadi, T.F. Yen, Energy Fuels 21 (2007) 1622.
[7] M.A. Safa, X.L. Ma, Fuel 171 (2016) 238–246.
[8] D. Piccininoa, I. Abdalghani, G. Bottaa, M. Crucianelli, M. Passacantando, M.L.D. Vacri, R. Saladino, Appl. Catal. B 200 (2017) 392–401.
[9] H.W. Yang, B. Jiang, Y. l. Sun, L. Hao, Z.H. Huang, L.H. Zhang, Chem. Eng. J. 306 (2016) 131–138.
[10] K.X. Lee, J.A. Valla, Appl. Catal. B 201 (2017) 359–369.
[11] E. Torres-García, A. Galano, G. Rodriguez-Gattorno, J. Catal. 282 (2011) 201–208.
[12] Y. Shi, G. Liu, B. Zhang, X. Zhang, Green Chem. 18 (2016) 5273–5279.
[13] C. Shi, W. Wang, N. Liu, X. Xu, D. Wang, M. Zhang, P. Sun, T. Chen, Chem. Commun. 51 (2015) 11500–11503.
[14] C.M. Granadeiro, S.O. Ribeiro, M. Karmaoui, R. Valenca, J.C. Ribeiro, B. de Castro, L.S. Cunha-Silva, S.S. Balula, Chem. Commun. 51 (2015) 13818–13821.
[15] G. Miao, D. Huang, X. Ren, X. Li, Z. Lia, J. Xiao, Appl. Catal. B 192 (2016) 72–79.
[16] L. Cedeño-Caero, H. Gomez-Bernal, A. Fraustro-Cuevas, H.D. Guerra-Gomez, R. Cuevas-Garcia, Catal. Today 133 (2008) 244–254.
[17] L. Cedeño Caero, J.F.A. Navarro, A. Gutierrez-Alejandre, Catal. Today 116 (2006) 562–568.
[18] Y. Chen, H.Y. Song, Y.Z. Lu, H. Meng, C.X. Li, Z.G. Lei, B.H. Chen, Ind. Eng. Chem. Res. 55 (2016) 10394–10403.
[19] H. Zhao, G.A. Baker, Q. Zhang, Fuel 189 (2017) 334–339.
[20] N. Wang, M. Duchamp, R.E. Dunin-Borkowski, S.Y. Liu, X.T. Zeng, X. Cao, Y. Long, Langmuir 32 (2016) 759–764.
[21] J.T. Zhu, A.B. Huang, H.B. Ma, Y.N. Ma, K. Tong, S.D. Ji, S.H. Bao, X. Cao, P. Jin, ACS Appl. Mater. Interfaces 8 (2016) 29742–29748.
[22] M. Gurvitch, S. Luryi, A. Polyakov, A. Shabalov, J. Appl. Phys. 106 (2009) 104504.
[23] C. Petchsingh, N. Quill, J.T. Joyce, D. Ní Eidhin, D. Oboroceanu, C. Lenihan, X. Gao, R.P. Lynch, D.N. Buckley, J. Electrochem. Soc. 163 (1) (2016) A5068–A5083.
[24] D. Alie, L. Gedvilas, Z. Wang, R. Tenent, C. Engtrakul, Y. Yan, S.E. Shaheen, A.C. Dillon, C. Ban, J. Solid State Chem. 212 (2014) 237–241.
[25] J. Zou, Y. Peng, H. Lin, J. Mater. Chem. A 1 (2013) 4250–4254.
[26] A.M. Makarevich, I.I. Sadykov, D.I. Sharovarov, V.A. Amelichev, A.A. Adamenkov, D.M. Tsymbarenko, A.V. Plokhih, M.N. Esaulkov, P.M. Solyankin, A.R. Kaul, J. Mater. Chem. C 3 (2015) 9197–9205.
[27] D. Li, M. Li, J. Pan, Y. Luo, H. Wu, Y. Zhang, G. Li, ACS Appl. Mater. Interfaces 6 (2014) 6555–6561.
[28] Y.F. Zhang, Y.F. Huang, J.C. Zhang, W.B. Wu, F. Niu, Y.L. Zhong, X.H. Liu, X. Liu, C. Huang, Mater. Res. Bull. 47 (2012) 1978–1986.
[29] D.H. Wang, N. Liu, J.Y. Zhang, X. Zhao, W.H. Zhang, M.H. Zhang, J. Mol. Catal. A: Chem. 393 (2014) 47–55.
[30] C.Z. Wu, J. Dai, X.D. Zhang, J. Yang, F. Qi, C. Gao, Y. Xie, Angew. Chem. Int. Ed. 49 (2010) 134–137.
[31] X. Cao, M.N. Thet, Y. Zhang, S.C.J. Loo, S. Magdassi, Q. Yan, Y. Long, RSC Adv. 5 (2015) 25669–25675.
[32] X.L. Li, J.F. Liu, Y.D. Li, Mater. Chem. Phys. 80 (2003) 222–227.
[33] M. Zhou, J. Bao, M. Tao, R. Zhu, Y. Lin, X. Zhang, Y. Xie, Chem. Commun. 49 (2013) 6021–6023.
[34] J.F. Xie, C.Z. Wu, S.L. Hu, J. Dai, N. Zhang, J. Feng, J.L. Yang, Y. Xie, Phys. Chem. Chem. Phys. 14 (2012) 4810–4816.
[35] Z. Hasan, J. Jeon, S. Jhung, J. Hazard. Mater. 205–206 (2012) 216–221.
[36] A. Bazyari, A. Khodadadi, A. Mamaghani, J. Beheshtianb, L. Thompsonc, Y. Mortazav, Appl. Catal. B 180 (2016) 65–77.
[37] L. Rivoira, V. Vallés, B. Ledesma, M. Ponte, M. Martínez, O. Anunziata, A. Beltramone, Catal. Today 271 (2016) 102–113.
[38] D.H. Wang, E.W.H. Qian, H. Amano, K. Okata, A. Ishihara, T. Kabe, Appl. Catal. A 253 (2003) 91–99.
[39] F. Mashio, S. Kato, Yuki Gousei Kagaku 26 (4) (1968) 367.
[40] K.Y. Tsai, T.S. Chin, H.P.D. Shieh, C.H. Ma, J. Mater. Res. 19 (2004) 2306–2314.
[41] X.G. Tan, T. Yao, R. Long, Z.H. Sun, Y.J. Feng, H. Cheng, X. Yuan, W.Q. Zhang, Q.H. Liu, C.Z. Wu, Y. Xie, S.Q. Wei, Sci. Rep. 2 (2012) 466.
[42] C. Leroux, G. Nihoul, G.V. Tendeloo, Phys. Rev. B 57 (1998) 5111–5121.